Investigation on multi-track multi-layer epitaxial growth of columnar crystal in direct laser forming

XuanTuoi Do[a)]

State Key Laboratory for Manufacturing Systems Engineering, Xi'an Jiaotong University, No. 28,
Xianning West Road, Xi'an 710049, China and Le Quy Don University, No. 100, Hoang Quoc Viet Street,
Hanoi 7EN-218, Vietnam

Dichen Li,[b)] Anfeng Zhang,[c)] Bin He,[d)] and Haiyang Zhang[e)]

State Key Laboratory for Manufacturing Systems Engineering, Xi'an Jiaotong University, No. 28,
Xianning West Road, Xi'an 710049, China

Tatkhoa Doan[f)]

State Key Laboratory for Manufacturing Systems Engineering, Xi'an Jiaotong University, No. 28,
Xianning West Road, Xi'an 710049, China and Le Quy Don Technical University, No. 100, Hoang Quoc Viet
Street, Hanoi 7EN-241, Vietnam

Direct laser forming has the advantage that the heat input is very much localized and it leads to large temperature gradient. Therefore, the solidification velocity can be controlled to stabilize the columnar crystal growth and to avoid the growth of equiaxed grains in the laser clad. Consequently, single crystal can be deposited onto a single crystal substrate. In this paper, DZ125L Ni based super-alloy was used for the experiment, the epitaxial growth of columnar crystal onto the substrate was characterized, and the epitaxial growth of columnar crystal in multi-track multi-layer deposition was obtained by analyzing the single cladding track characteristics and optimizing the technological parameters. The investigation is helpful for the approach to form 3D metal parts such as turbine blades, which require columnar crystal microstructure. © 2013 Laser Institute of America.

I. INTRODUCTION

Based on rapid prototyping and laser cladding technique, direct laser forming (DLF) is a novel layer additive manufacturing technology.[1–3] DLF supports many types of metal including stainless steel, Ni based super-alloys, cobalt-chrome, and Ti-6Al-4V titanium alloy.[4] By using DLF, dense metal parts can be fabricated directly from computer aided design (CAD) files line by line and layer by layer without using any tooling. The outstanding characteristics of DLF are high energy density, good controllability, compact cladding microstructure, few microscopic flaw, and high bonding strength. Additionally, there are many advantages in the technological process such as easy to realize automation, little pollution to the environment, no radiation, and low noise.[5,6]

In recent years, DLF has been a hot topic in the advanced manufacturing fields to repair expensive parts or to form high performance metal parts such as turbine blades, which are usually made by super-alloys and require directional columnar crystal microstructure. Actually, turbine blade can be formed by selective laser melting—SLM,[7] by direct metal deposition—DMD,[8] or by DLF.[9,10] However, the mechanical performance of the parts fabricated by the above mentioned methods has not been reported sufficiently. Recently, some researches into repairing, coating,[11–13] and fabricating[14] of directional columnar crystal Ni based super-alloy by DLF have been published, whereas all of them showed poor results. At present, forming columnar crystal 3D metal part by DLF still remains a great challenge.

DZ125L, designed in China for application in advanced gas turbine engines, is a high performance Ni based super-alloy. By far, there have been some investigations on DLF of DZ125L,[15,16] but no report on fabrication of DZ125L columnar crystal 3D samples. Using DZ125L for the experiment, and this paper systematically investigated the influence of the main technological parameters such as laser power, scanning speed, powder feeding rate on the characteristics of single cladding track, and the elementary unit in DLF. By analyzing the results and optimizing the technological parameters, the epitaxial growth of columnar crystal onto the substrate in the form of multi-track multi-layer was obtained. The result showed that DZ125L super-alloy 3D solid samples with columnar crystal microstructure can be fabricated by DLF.

II. EXPERIMENTAL PROCEDURE

A. Materials and equipments

The experiments were carried out by the system as shown in Fig. 1. The DLF process was performed by independently developed XJTU-I machines, which include a

---

[a)]Electronic address: dxtuoi76@gmail.com.
[b)]Electronic address: dcli@mail.xjtu.edu.cn.
[c)]Electronic address: anfengzh@mail.xjtu.edu.cn.
[d)]Electronic address: hb0035@hotmail.com.
[e)]Electronic address: ibelieve5310@126.com.
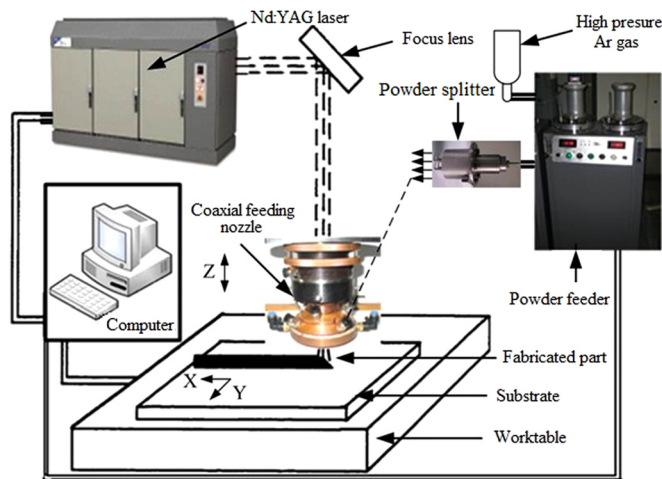[f)]Electronic address: doankhoactm@gmail.com.

FIG. 1. Schematic diagram of experiment setup.

FIG. 2. The tensile properties of DZ125L.

neodymium doped yttrium aluminium garnet (Nd:YAG) laser with a 1 kW maximum output power (wavelength 1063 nm, spot diameter of 0.5 mm, the laser beam is guided to the workstation through an optical fiber and focused by a lens system), a three-axis computerized numerical control (CNC) linkage worktable, a powder feeder with a coaxial feeding nozzle, and a gas protection device. The processing chamber of the system was protected from oxidation by argon gas.

The powder was DZ125L Ni based super-alloy with spherical shape and smooth surface. Additionally, the DZ125L particle size distributes from 30 to 60 μm, and the mean particle size is about 45 μm. The same material was used for the substrate, which was machined from single crystalline cast ingots with the $\langle 001 \rangle$ orientation normal to the surface, and its dimensions were 50 mm of the diameter and 3.5 mm of the thickness. Material compositions of the substrate and the powder are shown in Table I. The tensile properties of DZ125L are shown in Fig. 2.[17]

B. Processing

The powder was dried in a vacuum oven at 200 °C for 2 h to remove the moisture and to improve the flowability. The substrate was polished and then cleaned by acetone before being installed on the forming worktable and leveled. Single cladding tracks (20 mm in length) were prepared with different laser powers P, scanning speeds V, and powder feeding rates M_P (as shown in Table II). Three separate tracks were prepared with each parameter set of (M_P, P, V). Twenty sets of (M_P, P, V) were used, sixty separate tracks were prepared. The values of each parameter in the set of (M_P, P, V) were selected according to the
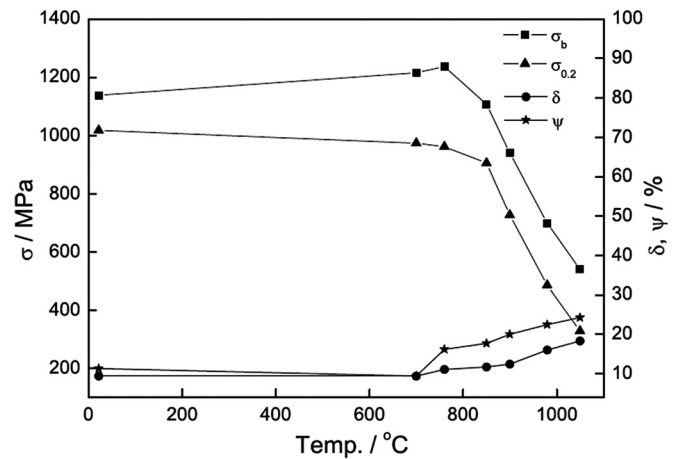
preliminary basic research. Multi-track one layer and multi-track multi-layer samples were clad based on the analysis of the single cladding track characteristics. Neither preheat nor postdeposition heat treatment of the deposited samples was applied. The samples were cut for characterization with wire electric discharge machining (EDM). All samples were mounted and prepared in accordance with standard metallographic procedures. The topography characteristics and the microstructure characteristics of each sample were analyzed using VH3000 optical microscope (made in Japan by the KEYENCE).

The cross section of each single track was characterized, after that the symbolic cross section of each technology parameter set was obtained. By analyzing the results, technological parameters that can make the epitaxial growth of columnar crystal in multi-track multi-layer deposition were optimized.

III. RESULTS AND DISCUSSION

A. The epitaxial growth of columnar crystal onto the substrate

After polishing and etching the samples, directional dendrite structure in the substrate was released. The refined dendrite structure in the deposit zone showed an epitaxial growth parallel with the substrate dendrite direction. The epitaxial growth also verified the nature of bonding at the interface to be metallurgical. Compared with the dendrite size of the substrate metal, the primary dendrite size in the deposit zone is approximately 50–70 times smaller.

TABLE I. Material compositions of the substrate and the powder (wt. %).

Material	C	Cr	Co	Mo	W	Al	Ti	Ta	B	Ni
Substrate	0.07	9.09	10.00	2.09	7.17	4.48	3.05	3.64	0.011	Balance
Powder	0.09	9.70	9.64	2.18	7.14	4.90	3.12	3.78	0.015	Balance

TABLE II. Technology parameters for single cladding tracks.

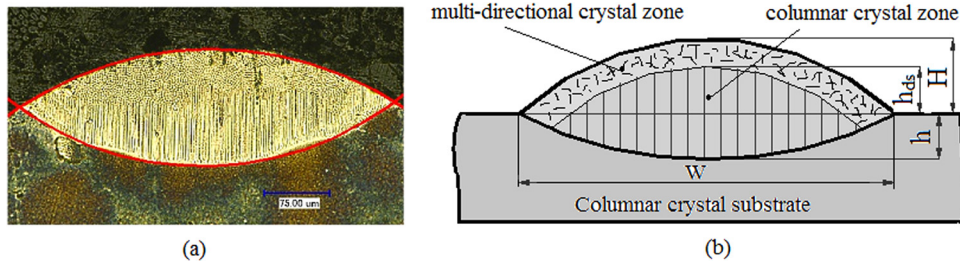|	
Powder feed rate M_P (g min^{-1})	4.9
Laser power P (W)	190, 210, 230, 250, 270
Scanning velocity V (mm s^{-1})	6, 8, 10, 12
Shielding gas rate (l min^{-1})	4
Protecting gas rate (l min^{-1})	6
Track number of each set of (M_P, P, V)	3

FIG. 3. Typical sketch of the cross section of single cladding track. (a) The typical sketch of the cross section of the cladding track; (b) the cladding track cross section morphology.

The experiment results showed the cross section of single cladding track with arc boundary shape. The typical sketch of the cross section of the cladding track is shown in Fig. 3(a). The cladding track cross section morphology is described with the cladding track width W (μm), the cladding track height H (μm), the remelted depth of the substrate h (μm), and the height (from the substrate surface) of columnar crystal zone h_{ds} (μm), respectively [as shown in Fig. 3(b)]. It

can be seen that both H and h reached their maximum at the center of the laser beam, and they decreased from the center to the side. It is consistent with the distribution laws of the laser beam energy and the powder stream. The cross section includes columnar crystal zone, which grows continuously from the substrate, and multidirectional crystal zone [Fig. 3(b)]. Not like H and h, the height of columnar crystal zone h_{ds} was not changed linearly from the center to the side,
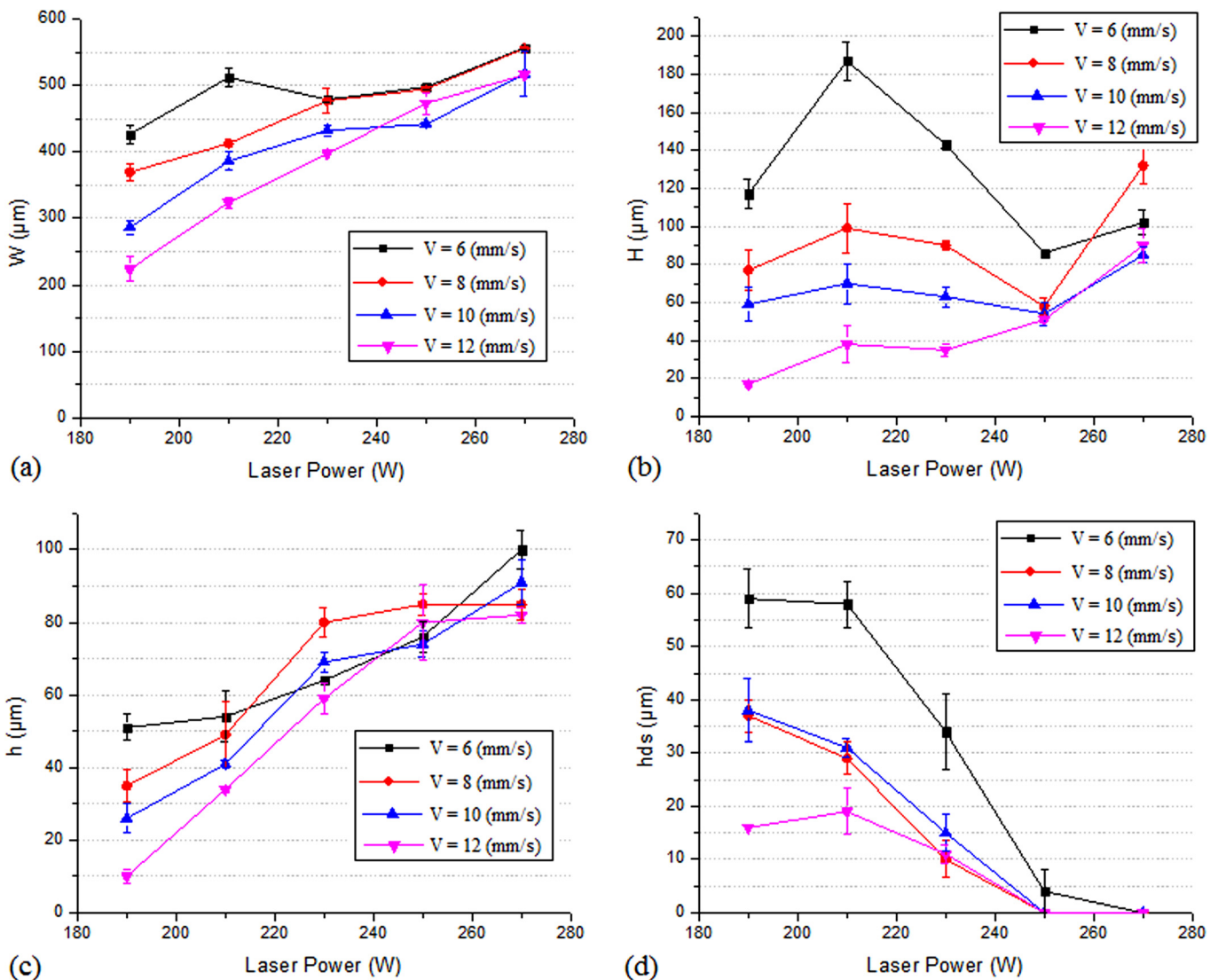

FIG. 4. Influence of the technological parameters on the single cladding track characteristics. (a) The cladding track width W, (b) the cladding track height H, (c) the remelted depth of the substrate h, and (d) the height of columnar crystal zone h_{ds}.
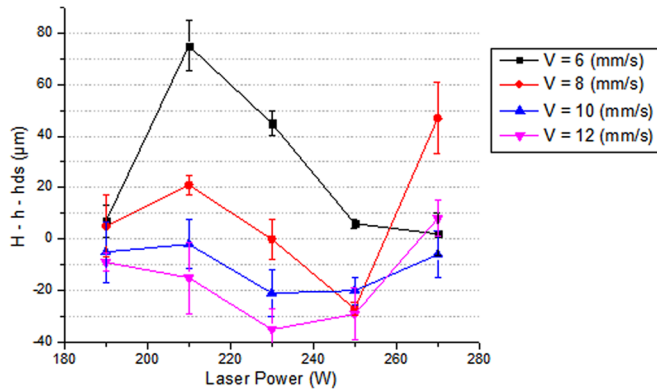
FIG. 5. The difference value of H-h_{ds}-h.

but it usually reached its peak at the central position. The side part of the cross section usually belongs to the multidirectional crystal zone. It can be explained that at the side part, the laser energy density is low, the remelted depth is very small, the heat is transferred quite quickly from the molten pool into the substrate by conduction, and the transferring direction is changed from normal to parallel with the substrate surface.

The morphology parameters of single tracks were measured after the experiment. From each set of (M_P, P, V), which was used for three separate tracks, three value sets of (W, H, h, and h_{ds}) were obtained. These values were then used in calculation to find out each mean value of W, H, h, and h_{ds}, which finally expressed by the diagrams in Figs. 4 and 5. It can be seen in Fig. 4 that with different technological parameters, single cladding track cross sections with different characteristics were released. The result showed that the increase in laser power P led to the increase in the cladding track width W and the remelted depth h [Figs. 4(a) and 4(c)]; the increase in laser power P led to the decrease in the height of columnar crystal zone h_{ds} [Fig. 4(d)]. The cladding track height H was relatively stable when the scanning speed is 8 or 10 mm s^{-1}, small when the scanning speed is 12 mm s^{-1} and big at the scanning speed of 6 mm s^{-1} [Fig. 4(b)]. The height of columnar crystal zone h_{ds} is

the most important parameter, and it must be relatively greater than zero to make the subsequent layer with an epitaxial growth parallel to the previous one. Figure 4(d) also indicated that laser power P should not be higher than 250 W.

Moreover, the dendrite layer (multidirectional crystal zone) and an interdendrite shrinkage should be thoroughly remelted to guarantee the densification and the epitaxial growth between the depositing layer and the previous one. It can be seen in Fig. 3(b) that the difference ($H-h_{ds}$) must be smaller than h, which means that the difference ($H-h_{ds}-h$) must be negative. The calculation result, which is shown in Fig. 5, indicated that the suitable condition is obtained when the scanning speed is 10 or 12 mm s^{-1} and laser power is less than 270 W. Low scanning speed of 6 or 8 mm s^{-1} (with laser power less than 230 W) is not suitable, and 8 mm s^{-1} scanning speed is suitable only when laser power is in range of 230–255 W.

B. The epitaxial growth of columnar crystal in multi-track cladding

Figure 6 shows the model of the remelted zone of the previous track and the substrate when the subsequent track clad according to the two tracks distance ΔX (the zone within the bold curves). Multi-track experimental results with different values of ΔX are shown in Fig. 7. It can be seen that with a big ΔX [Fig. 6(a)], the previous track was remelted only in the multidirectional crystal zone; therefore, the columnar crystal zone of the subsequent track could not grow continuously from the previous one [Fig. 7(a)]. The decrease in ΔX led to the increase of the remelted zone of the previous track. As ΔX reached up to a certain value, the remelted zone included both columnar crystal zone and multidirectional crystal zone of the previous track, and the epitaxial growth of columnar crystal from both the previous track and the substrate occurred (Figs. 6(b), 7(b), and 7(c)). Moreover, the columnar crystal zone between the previous and the subsequent tracks also developed in height with the decrease in ΔX [Fig. 7(c) compare with Fig. 7(b)].
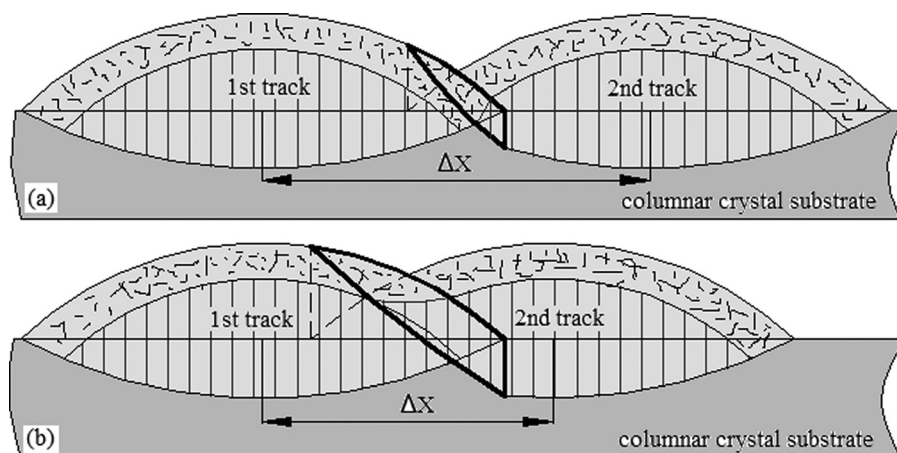

FIG. 6. Remelted zone according to the two tracks distance ΔX. (a) When ΔX is big; (b) when ΔX is suitable.
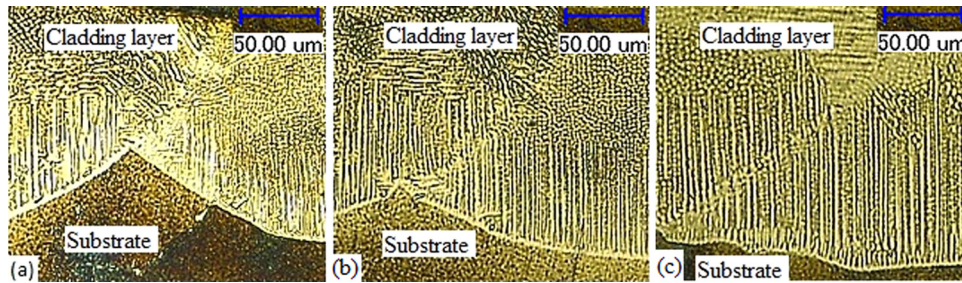
FIG. 7. Multi-track experimental results with different values of ΔX (mm). (a) $\Delta X = 0.40$, (b) $\Delta X = 0.34$, and (c) $\Delta X = 0.30$, and the other technological parameters were $P = 230$ W, $M_P = 4.9$ g min^{-1}, $V = 10$ mm s^{-1}.

C. DZ125L super-alloy 3D sample forming

From above analysis, we can see that by determining single cladding track characteristics, which were obtained by optimizing technological parameters through experiments, the epitaxial growth of columnar crystal can be obtained layer by layer onto the substrate. The results indicate that suitable laser power is in range of 210–250 W, scanning speed is 10 mm s^{-1}, and powder feeding rate is 4.9 g min^{-1}. Moreover, the epitaxial growth of columnar crystal can also be obtained track by track with the suitable value of ΔX. Based on the result, 3D solid samples were formed. Table III shows the used technological parameters.

The results showed that a strong metallurgical bonding has been achieved between the formed samples and the substrate. For the sample No. 1, the result showed the epitaxial growth of columnar crystal track after track in each layer (as shown in Fig. 8). However, Fig. 8 also shows some small zones (among layers, inside the black curves) are multidirectional crystal. It can be explained that due to the oscillation of the experimental system, the multidirectional crystal zone of cladding tracks of the previous layer was sometime not remelted completely by the subsequent layer deposition. Therefore, the columnar crystal of subsequent layer could not grow continuously from the previous one. The subsequent layer still showed columnar crystal structure above multidirectional crystal zones. It may be because of the high temperature gradient when the first layers were fabricated.

It is necessary to remove all the multidirectional crystal zones among layers to make the columnar crystal growing continuously. The microstructure of sample No. 2 is shown in Fig. 9 (perpendicular to the scanning direction (a) and parallel with the scanning direction (b) cross sections). With
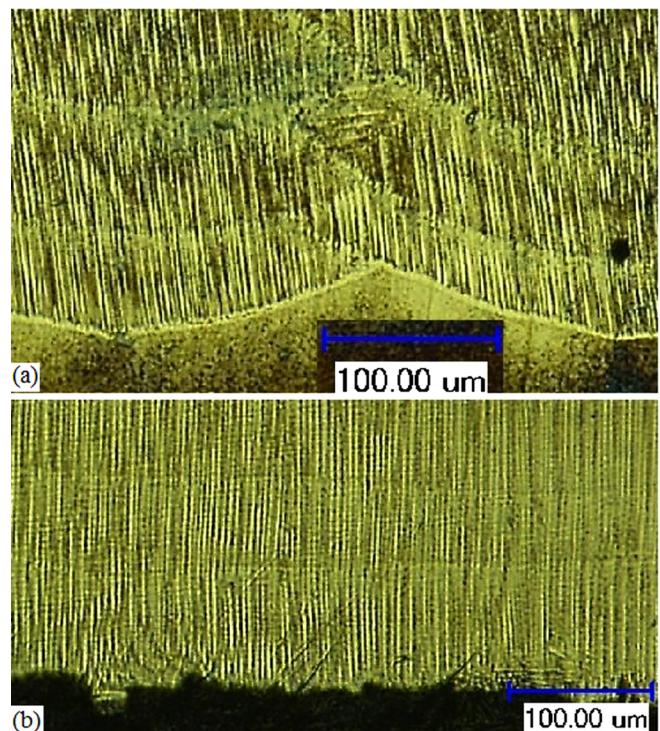

FIG. 8. Microstructure of sample No. 1.

FIG. 9. Microstructure of sample No. 2.

TABLE III. The technological parameters for 3D solid samples.

Technological parameters	Sample No. 1	Sample No. 2
Laser power P (W)	230	230
Scanning speed V (mm s^{-1})	10	10
Powder feeding rate M_P (g min^{-1})	4.9	4.2
Number of track	7	7
Number of layer	10	10
Standoff distance Δh (mm)	0.1	0.08
Two tracks distance ΔX (mm)	0.3	0.3
Shielding gas rate (l min^{-1})	4	4
Protect gas rate (l min^{-1})	6	6

suitable technological parameters (decrease in powder feeding rate and decrease in the standoff distance Δh), we can see that the epitaxial growth of columnar crystal onto the substrate in the form of line by line and layer by layer was obtained.

IV. CONCLUSIONS

By analyzing the crystallized characteristic of single cladding track and optimizing technological parameters, we can see that directional columnar crystal can grow continuously onto a columnar crystal substrate in the form of line by line and layer by layer in DLF. The result showed that 3D sample with directional columnar crystal is obtained when the multidirectional crystal zone of the previous track or layer is sufficiently remelted by the deposition of the subsequent one.

ACKNOWLEDGMENTS

[1]H. M. Wang and G. Duan, "Wear and corrosion behavior of laser clad Cr3Si reinforced intermetallic composite coatings," Intermetallics **11**, 755–762 (2003).

[2]H. Tan, J. Chen, F. Y. Zhang, X. Lin, and W. D. Huang, "Process analysis for laser solid forming of thin-wall structure," Int. J. Mach Tools Manuf. **50**, 1–8 (2010).

[3]K. Venkatakrishanan, N. R. Sivakumar, C. W. Hee, B. Tan, W. L. Liang, and G. K. Gan, "Direct fabrication of surface-relief grating by interferometric technique using femtosecond laser," Appl. Phys. A: Mater. Sci. Process **77**(7), 959–963 (2003).

[4]Wohlers Associates, Inc., Additive Manufacturing and 3D Printing State of the Industry, Annual Worldwide Progress Report No. ISBN 0-9754429-7-X, Wohlers report 2011.

[5]Y. P. Kathuria, "Some aspects of laser surface cladding in the turbine industry," Surf. Coat. Technol. **132**, 262–269 (2000).

[6]L. Sexton, S. Lavin, G. Byrne, and A. Kennedy, "Laser cladding of aerospace materials," J. Mater. Process. Technol. **122**, 63–68 (2002).

[7]L. Gordon, "Technique Melts Metal Powder to Build Aero Turbine Blades. Machine Design," **82**(10), 40 (2010).

[8]J. Choi, B. Dutta, and J. Mazumder, "Spatial control of crystal texture by laser dmd process," in *Supplemental Proceedings of Fabrication, Materials, Processing and Properties TMS, Vol. 1* (The Minerals, Metals, and Materials Society, 2009), pp. 405–413.

[9]Z. L. Lu, D. C. Li, Z. Q. Tong, Q. P. Lu, M. M. Traore, A. F. Zhang, and B. H. Lu, "Investigation into the direct laser forming process of steam turbine blade," Opt. Lasers Eng. **49**(9–10), 1101–1110 (2011).

[10]Z. L. Lu, A. F. Zhang, Z. Q. Tong, X. H. Yang, D. C. Li, and B. H. Lu, "Fabricating the steam turbine blade by direct laser forming," Mater. Manuf. Processess. **26**, 879–885 (2011).

[11]L. Leijun, "Repair of directionally solidified superalloy GTD-111 by laser engineered net shaping," J. Mater. Sci. **41**, 7886–7893 (2006).

[12]R. Vilar, E. C. Santos, P. N. Ferreira, N. Franco, and R. C. da Silva, "Structure of NiCrAlY coatings deposited on single-crystal alloy turbine blade material by laser cladding," Acta Mater. **57**, 5292–5302 (2009).

[13]M. Gäumann, C. Bezençon, P. Canalis, and W. Kurz, "Single-crystal laser deposition of superalloys: Processing-microstructure maps," Acta Mater. **49**, 1051–1062 (2001).

[14]F. Liping, H. Weidong, L. Xin, Y. Haiou, L. Yanmin, and Y. Jian, "Laser multilayers cladding experiment on the DD3 single crystal using FGH-95 powder: Investigation on the microstructure of single crystal cladding layer," Chin. J. Aeronaut. **15**(2), 121–127 (2002).

[15]G. Jiangbo, Z. Anfeng, L. Dichen, Z. Gangxian, L. Qiaopan, H. Bin, and L. Zhongliang, "Process research on DZ125L superalloy parts by laser metal direct forming," Chin. J. Lasers **38**(7), 0703004 (2011).

[16]D. Tatkhoa, L. Dichen, L. Bingheng, Z. Anfeng, H. Bin, and D. Xuantuoi, "Effect of scanning methods on the cracking of the DZ125L superalloy in laser direct metal forming," Chin. J. Lasers **39**(10), 1003002 (2012).

[17]E. Liu, S. Sun, G. Tu, Z. Zheng, X. Guan, and L. Zhang, "Tensile and fracture behavior of DZ68 Ni-base superalloy," J. Mater. Sci. Technol. **25**(6), 727–730 (2009).